**Electronic Supplementary Information**

# Artificial Nacre-like Paper Based on Noncovalent Functionalized Boron Nitride Nanosheets with Excellent Mechanical and Thermally Conductive Properties

Xiaoliang Zeng,‡[a] Lei Ye,‡[b] Shuhui Yu,[a] Hao Li,[b] Rong Sun*[a], and Jianbin Xu*[b] and Ching-Ping Wong[b]

[a]*Shenzhen Institutes of Advanced Technology, Chinese Academy of Sciences. Shenzhen, China. Fax: 86-755-86392299; Tel: 86-755-86392158; Email: rong.sun@siat.ac.cn*

[b]Department of Electronics Engineering, The Chinese University of Hong Kong, Hong Kong, China. Fax: 852-26035558 ; Tel: 852-39438297; Email: *jbxu@ee.cuhk.edu.hk*

‡Xiaoliang Zeng and Lei Ye contributed equally to this work.

**Contents:**

- Figure S1. TEM images of NF-BNNSs with (a) low and (b) high magnification.
- Figure S2. DLS result of NF-BNNSs water suspension.
- Figure S3. Raman spectra of raw h-BN and BNNSs.
- Figure S4. TGA curves of raw BN and NF-BNNSs.
- Figure S5. XRD patterns of NF-BNNSs-PVA paper and pure BNNSs paper.
- Figure S6. Optical images of NF-BNNSs-PVA paper and pure BNNSs paper before (left) and after (right) soaking in water for 24 h.
- Figure S7. TGA curves of NF-BNNSs-PVA papers.
- Figure S8. Stress-strain curves of the NF-BNNSs-PMMA papers as a function of PMMA contents.
- Figure S9. Typical DSC curves of blank, sapphire, and sample to calculate the CP of samples.
- Measurement of in-plane thermal conductivity.

- Table S1. Summary of the mechanical properties of the papers measured by tensile testing.
- Table S2. Comparison of mechanical properties of our artificial nacre with the natural nacre and the reported graphene and graphene oxide papers.
- Table S3. A summary of the detailed sample information and thermal properties.

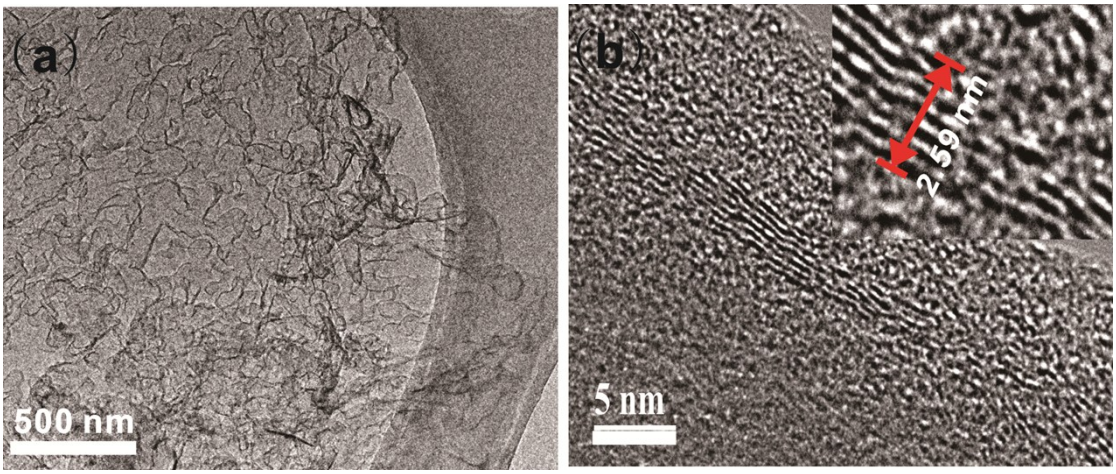


Figure S1. TEM images of BNNS with (a) low and (b) high magnification.

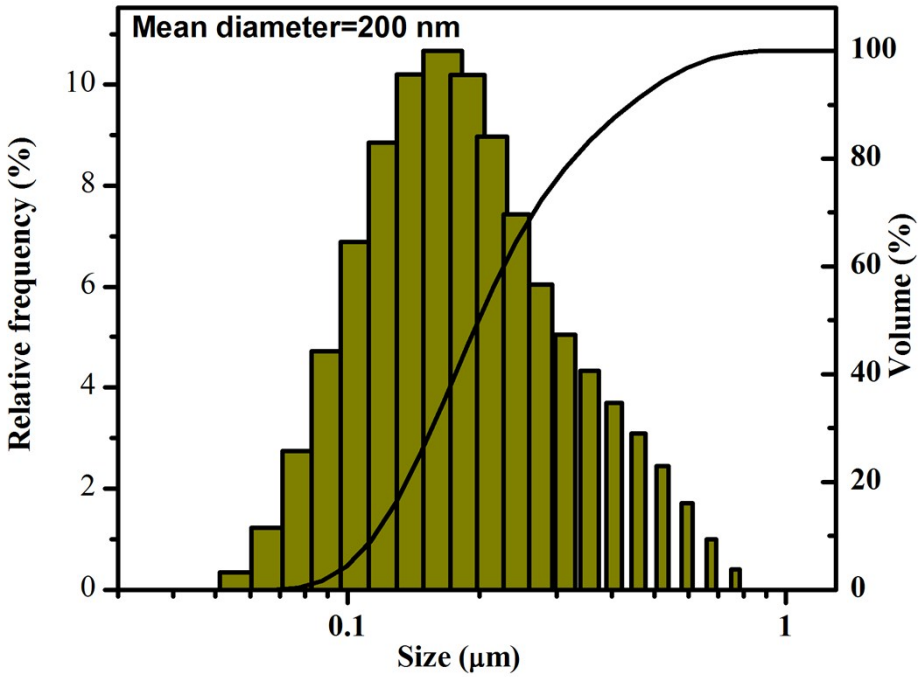


Figure S2. DLS result of NF-BNNSs water suspension.

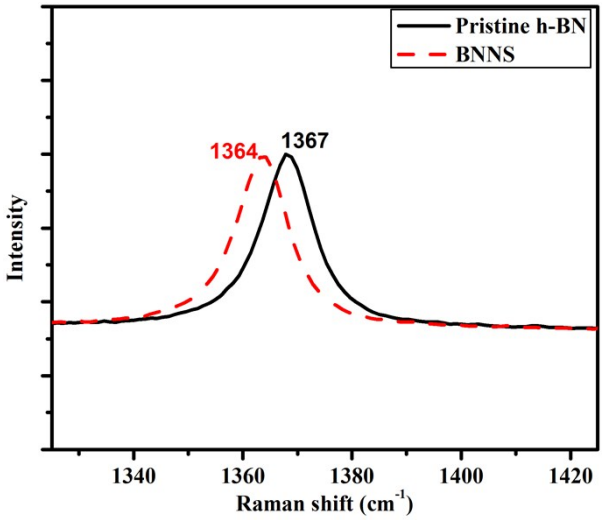


Figure S3. Raman spectra of pristine h-BN and BNNS.

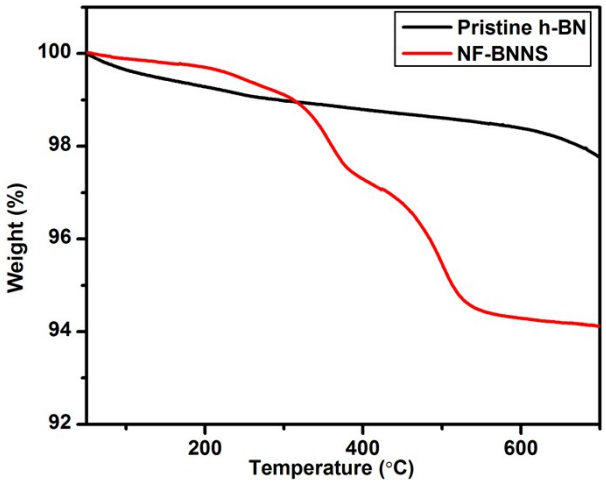


Figure S4. TGA curves of pristine BN and non-covalent functionalized BNNS (NF-BNNS).

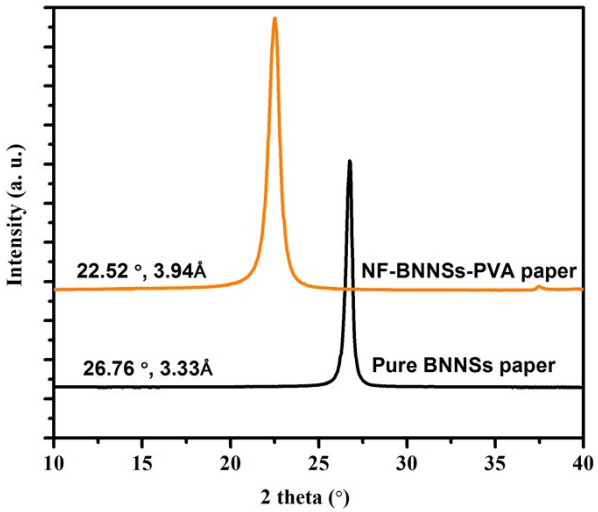


Figure S5. XRD patterns of NF-BNNSs-PVA paper and pure BNNSs paper.

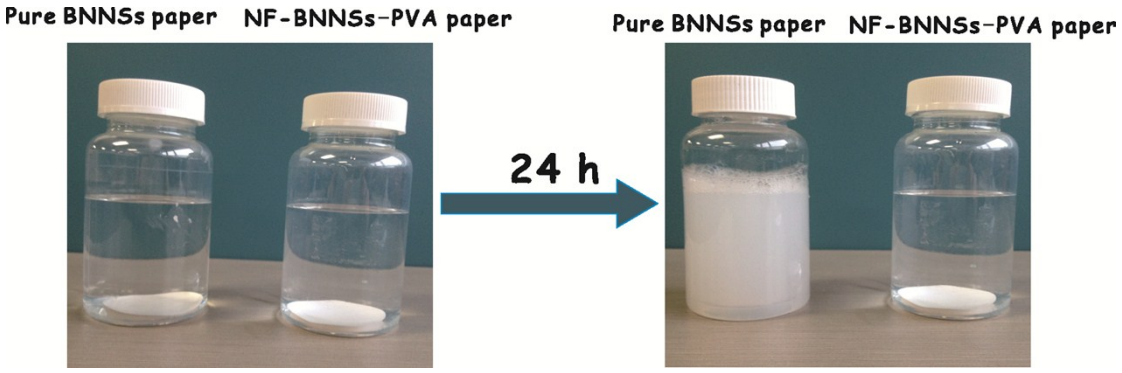


Figure S6. Optical images of NF-BNNSs-PVA paper and pure BNNSs paper before (left) and after (right) soaking in water for 24 h.

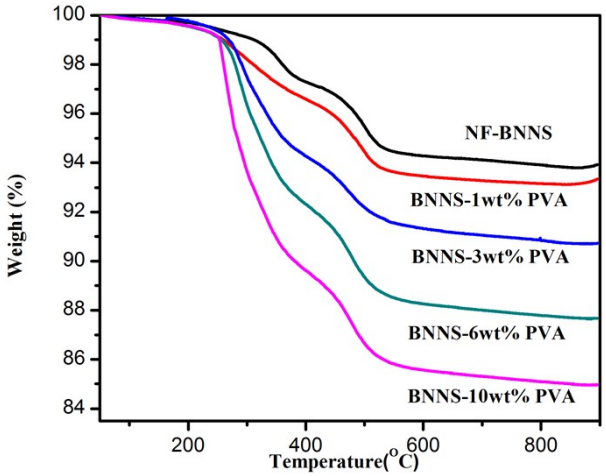


Figure S7. TGA curves of BNNS-PVA papers.

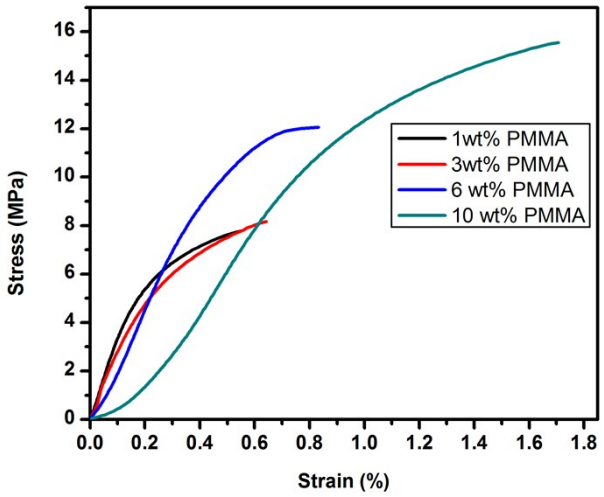


Figure S8. Stress-strain curves of the NF-BNNSs-PMMA papers as a function of PMMA contents.

Table S1. Summary of the mechanical properties of the papers measured by tensile testing.

| Samples | Tensile strength (MPa) | Young's modulus (GPa) | Toughness ($MJ.m^{-3}$) |
|---|---|---|---|
| Pure NF-BNNSs | - | - | - |
| NF-BNNSs-1wt% PVA | 7.0±0.5 | 3.9±0.4 | 0.021±0.002 |
| NF-BNNSs-3wt% PVA | 41.4±3.2 | 12.3±1.1 | 0.27±0.01 |
| NF-BNNSs-6wt%PVA | 125.2±5.1 | 15.7±0.7 | 2.37±0.2 |
| NF-BNNSs-10wt%PVA | 135.5±4.7 | 5.4±1.0 | 2.99±0.3 |
| NF-BNNSs-1wt% PMMA | 7.8±0.6 | 3.3±0.2 | 0.03±0.002 |
| NF-BNNSs-3wt% PMMA | 8.2±2.1 | 2.3±0.3 | 0.036±0.01 |
| NF-BNNSs-6wt% PMMA | 12.1±3.8 | 2.6±0.4 | 0.065±0.04 |
| NF-BNNSs-10wt% PMMA | 15.6±3.5 | 1.6±1.0 | 0.16±0.05 |

Table S2. Comparison of mechanical properties of our artificial nacre with the natural nacre and reported graphene and graphene oxide papers.

| System | 2D Materials loading | Strength (MPa) | Young's modulus (GPa) | Toughness ($MJ.m^{-3}$) | V ($\times 10^3$) | Year [Ref] |
|---|---|---|---|---|---|---|
| Natural nacre | 95 vol% | 80-135 | 60-70 | 1.80 | 11700 | 1988[1] |
| GO paper | 100 % | 120 | 31 | 0.24 | 892.8 | 2007[2] |
| GO-$PB^-$ | - | 8.4 | 4.2 | 0.01 | 0.35 | 2008[3] |
| GO-PVA | 72 wt% | 71.0 | 27.6 | 0.096 | 188.1.0 | 2010[4] |
| PGO-PEI | 50 wt% | 178.9 | 84.8 | 0.02 | 303.4 | 2013[5] |
| GO-Borate | 99.06wt% | 160 | 66.7 | 0.19 | 2027.7 | 2013[6] |
| RGO-PCDO | 93.5 wt% | 129.6 | 1.6 | 3.91 | 810.8 | 2013[7] |
| CRG-GO | 100 wt% | 5.5 | 0.51 | 0.08 | 0.22 | 2014[8] |
| Graphene-CF | 100 wt% | 15.2 | 6.5 | 0.03 | 2.96 | 2014[9] |
| Graphene-DOPA | - | 43.1 | 13.9 | 0.06 | 35.9 | 2014[10] |
| RGO-PVA | 50 wt% | 55.2 | 3.53 | 2.4 | 467.7 | 2014[11] |
| GTP–$Fe^{3+}$ | 94.4 wt% | 169.2 | 49.7 | 0.38 | 3195.5 | 2014[12] |
| NF-BNNS-PVA | 89 wt% | 125.2 | 15.7 | 2.37 | 4659.7 | Our data |

The toughness is estimated from the stress-strain curves in the references.
Abbreviations: GO paper, graphene oxide paper; GO-$PB^-$,GO-1-pyrenebutyrate; GO-PVA,GO-poly (vinyl alcohol); RGO-PVA, Reduced GO-PVA; PGO-PEI, Polydopamine-capped GO sheets- polyetherimide; GO-Borate, GO-$Na_2B_4O_7.10\ H_2O$; RGO-PCDO, RGO-10, 12-pentacosadiyn-1-ol; Graphene-DOPA, graphene-3,4-dihydroxy-phenylalanine; GTP-Fe, GO-tannic acid -$Fe^{3+}$ ions.

**Measurement of in-plane thermal conductivity.**

The in-plane thermal conductivity (λ) was calculated using Equation (S1):

$$\lambda = \rho.C_P.D \quad \text{(S1)}$$

Herein, ρ is the density, $C_p$ is the specific heat capacity, and $D$ is the thermal diffusivity of the composite BNNS paper.

The density (ρ) in Equation (S2) was obtained according to Equation (S2):

$$\rho = m/V \quad \text{(S2)}$$

Here $m$ and $V$ are the mass and volume of sample, respectively. The mass was available by weighing the round sample with a diameter of 25.4 mm using electronic precision balance. The volume was determined by the products of flake area and thickness of sample. The thickness was measured by micrometer caliper at specific pressure.

The specific heat capacity ($C_P$) was measured by DSC, according to ISO 1135-4:2005 Standard. The measurement was conducted using sapphire method according to Equation (S3):

$$C_P = C_P^{'}.\frac{m^{'}}{m}.\frac{y}{y^{'}} \quad \text{(S3)}$$

Here $C_p$ and $C_P^{'}$ are the specific heat of sample and standard specimen, respectively. $m$ and $m^{'}$ are the mass of the sample and sapphire, respectively. $y = DSC_{sample} - DSC_{blank}$ and $y' = DSC_{standard} - DSC_{blank}$. $DSC_{sample}$, $DSC_{blank}$ and $DSC_{standard}$ are the heat flow of the DSC curves corresponding to the sample, blank specimen, and standard specimen, respectively.

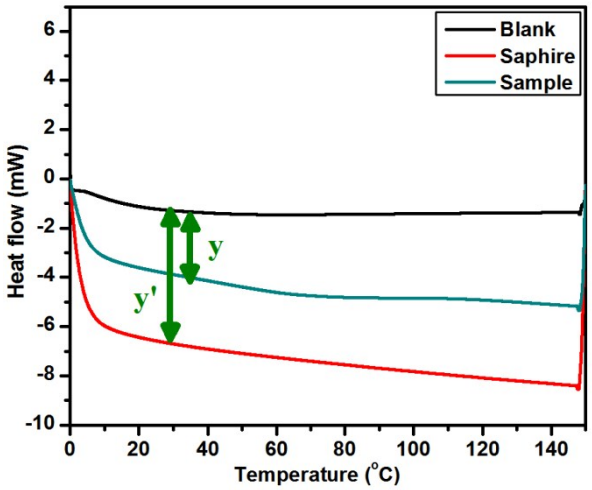


Figure S9. Typical DSC curves of blank, saphire, and sample to calculate the $C_P$ of samples.

Figure S9 shows typical DSC curves of blanks, sapphire, and sample to calculate the $C_P$ of sample. Three tests including blank test, sapphire test, and sample test were carried out in turn. Firstly, the base curve of DSC was achieved by the blank test. A sapphire was selected as reference sample with known $C_P$. Then the DSC curves, heat enthalpy change rate $dH/dT$ as a function of temperature $T$, of sample and sapphire were calibrated with the base curve. Comparing the DSC signal of sample with that of sapphire, $C_P$ of the being tested sample can be calculated.

The thermal diffusivity of all samples were further determined using Laser Flash Apparatus (NETZSCH LFA 447 NanoFlash) operated at room temperature. In this method, the test sample was cut into round shape with diameter of 25.4 mm, as the sample carrier is standard with fixed size. First, the sample was heated by light pulse, and then the resulting temperature rise at four different positions is measured using infrared detector. The thermal diffusivity was determined by analyzing the temperature-versus-time curve based on the following equation:

$$D = 0.1388.d^2.t_{1/2}^{-1} \quad \text{(S4)}$$

where, $D$ is the thermal diffusivity, $d$ is the thickness of the tested sample and $t$ is the diffusion time.

Table S3. A summary of the detailed sample information and thermal properties.

| Samples | $\rho$ (g $cm^{-3}$) | $C_P$ (J $g^{-1}$ $K^{-1}$) | $D$ ($mm^2$ $s^{-1}$) | $\lambda$ (W $m^{-1}k^{-1}$) |
|---|---|---|---|---|
| BN film | 1.04 | 0.64 | 6.024 | 4.02 |
| BN film/1%PVA | 1.19 | 0.69 | 6.497 | 5.33 |
| BN film/3%PVA | 1.29 | 0.70 | 6.653 | 6.01 |
| BN film/6%PVA | 1.32 | 0.72 | 7.384 | 6.95 |
| BN film/10%PVA | 1.35 | 0.70 | 4.76 | 4.50 |

References:


1. A. P. Jackson, J. F. V. Vincent and R. M. Turner, *P. Roy. Soc. B-Biol. Sci.*, 1988, **234**, 415-440.
2. D. A. Dikin, S. Stankovich, E. J. Zimney, R. D. Piner, G. H. B. Dommett, G. Evmenenko, S. T. Nguyen and R. S. Ruoff, *Nature*, 2007, **448**, 457-460.
3. Y. X. Xu, H. Bai, G. W. Lu, C. Li and G. Q. Shi, *J. Am. Chem. Soc.*, 2008, **130**, 5856-5857.
4. K. W. Putz, O. C. Compton, M. J. Palmeri, S. T. Nguyen and L. C. Brinson, *Adv. Funct. Mater.*, 2010, **20**, 3322-3329.
5. Y. Tian, Y. Cao, Y. Wang, W. Yang and J. Feng, *Adv. Mater.*, 2013, **25**, 2980-2983.
6. Z. An, O. C. Compton, K. W. Putz, L. C. Brinson and S. T. Nguyen, *Adv. Mater.*, 2011, **23**, 3842-3846.
7. Q. Cheng, M. Wu, M. Li, L. Jiang and Z. Tang, *Angew. Chem. Int. Edit.*, 2013, **52**, 3750-3755.
8. K. Shu, C. Wang, M. Wang, C. Zhao and G. G. Wallace, *J. Mater. Chem. A*, 2014, **2**, 1325-1331.
9. Q.-Q. Kong, Z. Liu, J.-G. Gao, C.-M. Chen, Q. Zhang, G. Zhou, Z.-C. Tao, X.-H. Zhang, M.-Z. Wang, F. Li and R. Cai, *Adv. Funct. Mater.*, 2014, **24**, 4222-4228.
10. D. Zhong, Q. L. Yang, L. Guo, S. X. Dou, K. S. Liu and L. Jiang, *Nanoscale*, 2013, **5**, 5758-5764.
11. B. Yuan, C. Bao, X. Qian, L. Song, Q. Tai, K. M. Liew and Y. Hu, *Carbon*, 2014, **75**, 178-189.
12. R.-Y. Liu and A.-W. Xu, *RSC Adv.*, 2014, **4**, 40390-40395.